Title

Insights from application of a hierarchical spatio-temporal model to an intensive urban black carbon monitoring dataset

Authors
Wai, Travis Hee
Apte, Joshua S
Harris, Maria H
et al.

Publication Date
2022-05-01

DOI
10.1016/j.atmosenv.2022.119069

Insights from Application of a Hierarchical Spatio-Temporal Model to an Intensive Urban Black Carbon Monitoring Dataset

Travis Hee Wai[1], Joshua S. Apte[2,3], Maria H. Harris[4], Thomas W. Kirchstetter[2,5], Christopher J. Portier[4], Chelsea V. Preble[2,5], Ananya Roy[4], and Adam A. Szpiro[6]

[1] Department of Medicine, Division of Pulmonary, Critical Care, and Sleep Medicine, University of Washington, Seattle, WA

[2] Department of Civil and Environmental Engineering, University of California, Berkeley, Berkeley, CA

[3] School of Public Health, University of California, Berkeley, Berkeley, CA

[4] Environmental Defense Fund, Washington, DC

[5] Energy Technologies Area, Lawrence Berkeley National Laboratory, Berkeley, CA

[6] Department of Biostatistics, University of Washington, Seattle, WA

Abstract

Existing regulatory pollutant monitoring networks rely on a small number of centrally located measurement sites that are purposefully sited away from major emission sources. While informative of general air quality trends regionally, these networks often do not fully capture the local variability of air pollution exposure within a community. Recent technological advancements have reduced the cost of sensors, allowing air quality monitoring campaigns with high spatial resolution. The 100×100 black carbon (BC) monitoring network deployed 100 low-cost BC sensors across the 15 km^2 West Oakland, CA community for 100 days in the summer of 2017, producing a nearly continuous site-specific time series of BC concentrations which we aggregated to one-hour averages. Leveraging this dataset, we employed a hierarchical spatio-temporal model to accurately predict local spatio-temporal concentration patterns throughout West Oakland, at locations without monitors (average cross-validated hourly temporal R^2=0.60). Using our model, we identified spatially varying temporal pollution patterns associated with small-scale geographic features and proximity to local sources. In a sub-sampling analysis, we demonstrated that fine scale predictions of nearly comparable accuracy can be obtained with our

modeling approach by using ~30% of the 100x100 BC network supplemented by a shorter-term high-density campaign.

1 Introduction

Short-term and long-term exposure to particulate air pollution, including black carbon (BC), is associated with adverse health effects[1]**.** Studies of short-term pollutant-health associations still often rely on centrally located regulatory monitors to estimate pollutant exposure for each study participant in the region[2,3]. However, concentrations can vary widely across a given area, such that a single measurement may not best describe population exposures everywhere, leading to possible biases in the estimates of health effects or identification of those most at risk. Our objective is to predict the spatially varying temporal patterns of BC concentrations in West Oakland during the summer months of 2017, a time that corresponds with intensive air pollutant monitoring in the area. Such predictions are of significant interest for use in a wide variety of applications, including epidemiological studies, as they allow researchers to calculate individual-specific short-term and long-term exposures based on finely resolved location information. From the perspective of air quality management and emissions control, more targeted management strategies such as regulatory agencies identifying times of day when areas are most affected by pollution might be possible. Vulnerable residents may be advised of times of day or week when they should be most cautious about spending time outdoors.

A number of approaches have been employed to predict intra-urban air pollution levels based on ground-level monitoring data[4,5]. Land-use regression (LUR) fits the exposure surface to a linear model with a large number of geographic information system (GIS) covariates[6], often using a combination of scientific and statistical learning techniques to reduce dimension of the covariate space[7–11]. Kriging models use a spatial random effect to construct a smooth prediction surface that predicts concentrations at unmonitored locations using an optimal weighted sum of nearby observations[12]. Researchers often combine LUR and kriging in a universal kriging (UK) that optimally combines regression and smoothing to improve prediction accuracy[7,13,14]. Recent advances in mobile monitoring technology and implementation have made comprehensive data-only spatial mapping an option in some areas, and in some cases LUR models have been trained on mobile monitoring data[15–18]. Spatiotemporal air pollution models combine LUR or UK with models for spatially varying temporal trends to accommodate temporally sparse data and to predict both spatial and temporal air pollution patterns in an urban environment. These models have been successful, especially at temporal scales of 1-2 weeks, although data availability is a limiting constraint[19–21].

Current reference-grade BC monitors cost ~$25,000, which places an economic constraint on the number of monitors that can be deployed in a network. To address this barrier, Caubel et al.[22] developed a new, low-cost BC sensor with similar precision and accuracy as existing commercial aethalometers based on the filter-based absorption photometry technology. With these low-cost BC sensors, it was possible to monitor BC concentrations with much greater spatial resolution by creating a dense sensor network across the community of West Oakland, California, a neighborhood surrounded by major highways and close to regional seaport and rail facilities. As part of the West Oakland Community Air Quality Study, the 100×100 Network deployed BC sensors across 100 locations in this community for 100 days from May 19 to August 26, 2017[23]. This measurement campaign produced a rich dataset of highly resolved BC concentrations in both space and time that we leverage in our modeling effort.

Maintaining a large network of sensors can be difficult in practice, operationally intensive, and susceptible to equipment failure or loss. The 100×100 BC Network achieved an 84% success rate at capturing valid hourly BC concentration measurements[23]. By the end of the 100 days of deployment, over 30 samplers were no longer operating, which enabled us to assess prediction accuracy of our spatio-temporal model subject to realistic maintenance and reliability constraints. A notable strength of our spatio-temporal model is its ability to leverage spatio-temporally sparse observations to improve predictions over the entire modeling period, as was similarly observed with the ability of a spatial only universal kriging model to leverage mobile monitoring data to predict spatial patterns BC concentrations across West Oakland[15].

In this paper, we use a spatio-temporal model to predict fine scale variation in BC concentrations across West Oakland, CA during part of the 100×100 Network monitoring period. We also subsample our dataset to evaluate how prediction accuracy is affected by monitor dropout patterns and to evaluate the implications of using a less dense monitoring network, possibly supplemented with a dense network over a shorter period.

2 Methods

2.1 Monitoring Data

The measurement sites, data quality assurance methods, and temporal and spatial variability of observed BC concentrations by different land use types in the 100×100 BC Network have been reported previously[23] and are summarized here. The 100×100 Network deployed 100 monitors throughout West Oakland outside of homes, local businesses, community organizations, and schools, and adjacent to the Port of Oakland. To verify sensor precision, nine network sites had sensors collocated in pairs and all sensors were calibrated based on 2–7 days operation collocated with a commercial BC instrument. Hourly average BC concentrations were calculated by averaging validated 1-minute averages, after correction for a filter loading artifact and errors in sample flow rate measurements. Due to the above-described equipment failure issues, an increasing number of sites were left unmonitored over the course of the 100 days. While 87% of potential hourly BC concentration measurements were successfully collected during the first 74 days of monitoring from mid-May to July, only 66% of were recorded during the last 26 days of monitoring in August. We primarily focused on analyzing data from June and July due to concerns that pollutant patterns at the end of May might have been qualitatively different from the summer seasonal patterns observed in June and July and due to data completeness limitations in August. As described later in this section, we utilized the pattern of data missingness (i.e., missing observations) in August to help assess how well our modeling approach would perform in a scenario with significant monitor dropout.

2.2 Hierarchical Spatio-Temporal Model

We used a hierarchical spatio-temporal model to predict time varying concentrations of BC at unmeasured locations in West Oakland[19,20,24,25]. Since the data tend to have heavy right tails and appear log-normally distributed, all modeling was done on the log-transformed scale to improve model fit. Prediction accuracy evaluation statistics were calculated on the back-transformed concentration scale. The spatio-temporal field is conceptualized as being comprised of location-specific temporal trends, where the trend at each location is the sum of the area-wide average (i.e., a time-series that is spatially constant across the domain) and a linear combination of two temporal basis functions. We included two temporal basis functions, $f_1(t)$ and $f_2(t)$, which were derived from the 100×100 Network data by first filling in missing values using an expectation-maximization-like approach[26] and applying cubic smoothing splines to the first two singular vectors. Preliminary exploratory analysis showed that including two temporal basis functions balanced model fit with interpretability of the temporal trends.

The full hierarchical spatio-temporal model can be written as

$$\log\big(\mathrm{Y}(\mathrm{s},\mathrm{t})\big) = \mu(\mathrm{s},\mathrm{t}) + \nu(\mathrm{s},\mathrm{t})$$

where $\log(\mathrm{Y}(\mathrm{s},\mathrm{t}))$ is the log-concentration of black carbon at site s for time t and

$$\mu(\mathrm{s},\mathrm{t}) = \eta(\mathrm{t}) + \beta_0(\mathrm{s}) + \beta_1(\mathrm{s})\,\mathrm{f}_1(\mathrm{t}) + \beta_2(\mathrm{s})\,\mathrm{f}_2(\mathrm{t}).$$

The location-specific coefficients for the temporal basis functions (including the intercept) are $\beta_\mathrm{i}(\mathrm{s})$ for $i = 0, 1, 2$, and $\eta(\mathrm{t})$ represents the area-wide average derived by averaging all monitoring data at each time t. The spatial structure of each $\beta_\mathrm{i}(\mathrm{s})$ is modeled by universal kriging, with regression on spatial covariates X_i with coefficients α_i in the mean model and normally distributed residuals with exponential covariance structure $\Sigma(\theta_i)$ that accounts for spatial correlation, i.e., $\beta_\mathrm{i}(\mathrm{s}) \sim N(\mathrm{X}_\mathrm{i}\alpha_\mathrm{i}, \Sigma(\theta_{\beta_\mathrm{i}}))$. The β_i-fields are independent of each other, and the exponential covariance function is parameterized by $\theta_\mathrm{i} = (\rho_\mathrm{i}, \sigma_\mathrm{i}^2, \tau_\mathrm{i}^2)$ with correlation range ρ_i, partial sill σ_i^2, and nugget τ_i^2. Finally, $\nu(\mathrm{s},\mathrm{t})$ represents temporally independent spatial residual fields with exponential correlation structures that account for short-term events such as meteorology affecting large subsets of the domain at any given time.

We calculated over 900 geographic information system (GIS) covariates to use in the model including proximity measures (distance to nearest major road, intersection, truck route, railway, railyard, coastline, airport, and port) and buffer measures (major road length, truck route length, land-use category, long-term vegetation index, population density, and emission sources). Following[19], GIS covariates with little to no variation or those that are highly skewed were removed from the modeling process. Specifically, any variables with *(a)* missing values, *(b)* >80% identical values, or *(c)* >2% more than 5 standard deviations (SD) from the mean were removed. Additionally, *(d)* any variables that describing land use at distances >5 km were removed, since the area of interest is only ~15 km^2. Because of the high dimensionality of the geographic covariates, we used principal component analysis (PCA) on the GIS covariates and selected the first two principal components to use as spatial covariates in our model.

This model is essentially the same model that was developed and applied in the MESA Air study[19] at the hourly rather than two-week timescale, with two significant changes that we made based on preliminary analyses of this dataset. One is that we explicitly include the area-wide average $\eta(t)$ in our model since there is a very strong shared temporal pattern at the hourly time scale. The other change is that we use PCA for dimension reduction of GIS covariates rather than partial least squares (PLS).

2.3 Model Estimation and Evaluation

Parameter estimation was performed using the SpatioTemporal package in R and optimization by restricted maximum likelihood (REML)[25]. Model accuracy was assessed by leave-one-site-out cross-validation. Let $Y(s,t)$ be the observed BC concentration at location s at time t and $\hat{Y}(s,t)$ the associated cross-validated predictions. At each location s, we calculated a measure of cross-validated prediction accuracy as follows:

$$R_{CV}^2 = max(0{,}1 - MSE/Var_{obs})$$

where

$$MSE = \frac{1}{t}\sum_{i=1}^{t}\left(Y(s,t_i) - \hat{Y}(s,t_i)\right)^2$$

$$Var_{obs} = \frac{1}{T}\sum_{i=1}^{T}\left(Y(s,t_i) - \frac{1}{T}\sum\nolimits_{j=1}^{T} Y(s,t_j)\right)^2$$

Like the squared Pearson correlation coefficient, a value of 1 denotes perfect correlation. Additionally, the measure penalizes for bias and scaling errors whereas the Pearson correlation coefficient does not.

We calculated these measures for two timescales, namely the hourly values over the entire period of June and July and the consolidated calendar week hourly values averaged over all weeks in June and July; i.e., for the latter, we collapsed the observed and predicted time series at each location to single average values for each hour of each day of the week (see bottom-right panel of Figure 1.

Due to the computational burden associated with solving the nonlinear REML optimization problem[25], we carried out this step only once on all of the data and used the resulting covariance parameter estimates to compute leave-one-out cross-validated R^2 for each site individually. There is minimal potential for overfitting because only the covariance (smoothing) parameters were estimated outside of the cross-validation loop, while regression coefficients were re-estimated for each cross-validation set. The estimated parameter values are reported in Table S-1.

2.4 Simulating Less Intensive Monitoring

Significant data collection dropout occurred during the month of August, so we used only the June and July data for model fitting and evaluation. We conducted a sensitivity analysis to assess the impact on prediction accuracy if we had elected to also include data from August and make predictions during that time period. We started with the fully observed 100×100 dataset in June and July and then created a missingness pattern in July that matched the observed missingness pattern in August. Using this version of the dataset to represent a monitoring campaign with dropouts, we fit the spatio-temporal model and estimated the observed pollutant concentrations at each location using leave-one-out cross-validation. We compared cross-validated prediction accuracy in July using the model with artificially created missingness against the original model, which used all available observations to understand how realistic long-term maintenance and logistical issues would affect prediction accuracy.

We also evaluated how the number of continuously operating monitors and their placement impact predictive accuracy of the spatio-temporal model by systematically subsampling our dataset to simulate estimates from a smaller network. We considered having 5, 10, 20, and 30 continuously operating monitors and sampled these monitors in three different ways:

1. Simple random sampling ("Random"): Randomly sampled k monitors with equal probability.
2. Stratified random sampling by GIS covariates ("GIS Covariates"): Clustered monitors at locations with similar local characteristics by using principal components of their GIS covariates in a k-means algorithm and then from each of the k clusters, randomly selected a monitor with equal probability.
3. Stratified random sampling by location ("Space Filling"): Clustered monitors spatially by first using a space-filling design to select k centers and then assigned monitors to clusters by distance. Monitors are then randomly selected from each of the k clusters with equal probability.

For each of these subsampling approaches, we considered one scenario where only the smaller number of continuously functioning monitors is available ("Long-Term Monitors Only") and another where these monitors were supplemented by a larger number of monitors in June only by including all available data from the 100×100 campaign in June ("Long-Term Monitors + Supplementation in June"). For each of these, we evaluated prediction accuracy of the spatio-temporal model on July data at all 100×100 locations.

3 Results

3.1 Monitoring Data

The spatial and temporal patterns of BC in West Oakland are described extensively elsewhere[15,23,27]. Briefly, key spatial features that are apparent in the 100x100 and mobile monitoring data include elevated levels near Interstate 880, along the major truck routes of the Port of Oakland, and near industrial clusters, with lower areas within predominantly residential zones. Temporal patterns vary across the domain and differ between weekdays and weekends. Weekday patterns broadly are characterized by a peak concentration during the morning rush hour, declining levels over the afternoon owing to increased atmospheric mixing, a less prominent evening peak, and lower levels in the late night and very early morning.

3.2 Model Description

We first look at components of the spatio-temporal models individually to describe the systematically varying spatial and temporal patterns. The area-wide average is shown in red, and two temporal trend functions are shown in green and blue in Figure 1. The top panel shows every hour throughout June and July. The bottom four panels show more interpretable versions consolidated to four different time scales: average diurnal 24-hour weekday, average diurnal 24-hour weekend day, average for each day of the week, and average for each hour during a typical week. In each panel, the red line shows the absolute value of the area-wide average concentration, and the green and blue lines show the relative differences compared to the area-wide average, with values < 0 equal to lower than area-wide average concentrations and values > 0 equal to greater than area-wide average concentrations.

The area-wide average concentration rises throughout the morning until 9 AM on weekdays, then slowly decreases throughout the day reaching its minimum value around 2 AM. On the weekends, there is a different pattern, with low concentrations throughout the day that slightly increase around 6 PM. On average, concentrations are lower on weekends and higher on weekdays, with some variation in diurnal patterns between days of the week. The first temporal basis function describes a pattern where concentrations are higher than the area-wide average from early morning until late in the afternoon on weekdays, with a peak around 9 AM. Concentrations at locations with a positive coefficient for the first temporal basis function are slightly below the area-wide average after 5 PM until midnight on weekdays, and well below the area-wide average all day on weekends. The second temporal basis function also shows an increase on weekdays but shifted later in the day, where concentrations are higher than the area-wide average from 7 AM until 8 PM. The above area-wide average concentration increases throughout the morning until about 1 PM, then slowly decreases over the afternoon. After 8 PM, this temporal basis function shows concentrations as below the area-wide average until the morning, with a minimum around 1 AM. On weekends, concentrations are higher than the area-wide average from 1 PM to 2 AM and are lower than the area-wide average during the other hours of the day.

Empirical estimates of the β-fields at locations with monitors are shown in Figure 2 along with their predicted values across West Oakland, and supplementary Figure S-1 shows cross-validated predictions of the empirical values of the β-fields. Locations in the southern part of West Oakland, especially the southeast corner downwind of major freeways and port activities, are associated with higher coefficient estimates for the β_0-field. This suggests that these areas have higher concentrations in general compared to the area-wide average. The β_0-field models the temporal average of log-transformed BC concentrations, so the difference in predicted values between the highest and lowest areas of the map in Figure 2 corresponds to a seven-fold difference in absolute concentrations.

Areas where the β_1-field are highest correspond to sites characterized as *port* and *truck routes* in Caubel et al. (2019)[23], and locations with lower coefficients align with locations described as being *residential* or *upwind* in Caubel et al. (2019)[23]. This is consistent with the fact that the first temporal basis function indicates concentrations higher than the area average during early morning hours, especially on weekdays when the port area is most active. The β_2-field is generally higher at industrial and residential sites in the northeast corner of West Oakland and lower in residential sites in the southwest corner of West Oakland. It is also high around the northern section of I-880 that feeds into I-80. The second temporal basis function is associated with higher than average concentrations starting in late-morning on weekdays and a modestly decreasing trend later in the week, potentially influenced by industrial sources during weekday business hours.

3.3 Prediction Accuracy

To demonstrate how the spatio-temporal model can improve fine-scale variation estimates across the region using temporal basis functions, we first compare the cross-validated predicted trends and the area-wide average to the actual observed trends for two example sites. Figure 3 shows the case study locations for this analysis, residential monitor 35 (R35) and truck route monitor 75 (TR75). While these monitors are located just three blocks apart and near the same arterial road, the average concentrations and temporal patterns at these two sites are different; monitored concentrations at TR75 are up to 0.5 $\mu g\ m^{-3}$ higher than the area-wide average, whereas monitored concentrations at R35 are similar to the area-wide average but with a lower weekday morning peak. Predicting concentrations by the area-wide average at these locations results in poor prediction accuracy, as measured by temporal R_{CV}^2 on the consolidated hour of week time scale (0.00 and 0.19 for R35 and TR75, respectively). Predictions from the spatio-temporal model at these two locations are much more accurate, with temporal R_{CV}^2 values on the consolidated hour of week time scale of 0.89 and 0.70 for R35 and TR75, respectively.

Overall, prediction accuracy for the spatio-temporal model varies across sites and depending on the temporal scale (Figure 4). Overall, the prediction accuracy is fair to good for locations near the port, with many of the most accurately predicted sites located in the northwest section of West Oakland. The mean temporal R_{CV}^2 is 0.60 for all hourly measurements over June and July and 0.58 for the consolidated hour of week time scale. These compare favorably to the corresponding values of 0.40 and 0.47 for the hourly and consolidated hour of week metrics, respectively, from using just the area-wide average to predict concentrations at all sites rather than predictions from the spatio-temporal model. Using a single well-sited monitoring location to represent the entire area would perform similarly to the area-wide average. On a site-by-site basis, using the spatio-temporal model yields a noticeable overall improvement in prediction accuracy at 72% of the observed sites over the area-wide average, showing the spatio-temporal model can capture fine scale gradients that would not be captured by the area-wide average.

3.4 Model Performance with Monitor Dropouts

To evaluate the effect of monitor dropouts like those experienced in August, a 30% dropout rate was simulated for the month of July. Predictions from this "masked" July dataset were compared to the full model run with all available June and July data. Using the full dataset shows a small, but noticeable improvement (Figure S-2, Figure S-3). The magnitude of this improvement is small and suggests that the effect of monitor dropouts, as observed in August, do not significantly impact prediction accuracy when using the spatio-temporal model. Based on these results, we expect that if the spatiotemporal model were fit using the entire 100×100 dataset (June–August), predictions for the August period would not be substantially less accurate than those for June and July, despite the higher missingness in monitoring data in August.

3.5 Systematic Subsampling Results

Results from the subsampling studies are shown in Figure 5, comparing mean temporal R^2_{CV} for the consolidated hour of week time scale in July. It does not appear that the method used to subsample monitor locations significantly impacts performance of the model. For a small number of continuously operating monitors such as 5 or 10, the spatio-temporal model predictions are less accurate than predicting based only on only the area-wide average, while with 20 or more continuously operating monitors the spatio-temporal model predictions consistently improve on the area-wide average. Adding more intensive short-term monitoring in June only (i.e., including all 100×100 monitors during that period) leads to an improvement regardless of the number of continuously operating monitors. This indicates that the model leverages data from the more intensive monitoring campaign in June to accurately predict concentrations in July when there were fewer monitors. Overall, our subsampling study suggests that 30 continuous monitors supplemented by a short-term, high-density monitoring campaign would allow us to construct a spatio-temporal model with prediction accuracy approaching that obtained with the full dataset. Performance is similar when the 30 monitors are selected at random compared to selecting them to representatively span the GIS covariate distribution or spatial distribution of the full dataset.

4 Discussion

By using a flexible, hierarchical spatio-temporal model with monitoring data from the 100×100 BC network, we were able to capture fine-scale differences in BC concentrations across

West Oakland. Our model predictions are significantly more accurate than what could be obtained by treating the pollution surface as spatially uniform and predicting the time series at each location based on data from a single well-placed regulatory monitor that might be found in a typical urban area, (mean temporal R^2s 0.60 and 0.40, respectively). We are aware of one other paper that attempted to model urban BC concentrations on an hourly timescale[21], with mixed success. A direct comparison is not possible because we report spatially varying temporal prediction accuracy, while Dons et al. (2013)[21] report spatial prediction accuracy for one hour averages. While comparisons with spatiotemporal predictions of other pollutants would also be informative, we are not aware of papers that have reported spatially varying temporal prediction accuracy as in our study. In addition to prediction accuracy, an important strength of the spatio-temporal model is its ability to help identify interpretable spatial patterns in temporal variation. For example, locations with larger positive values of the β_1 coefficient for the first temporal trend have relatively high weekday morning concentrations and tend to include sites identified in Caubel et al. (2019)[23] as associated with port activity. Similarly, locations with larger positive values of the β_2 coefficient for the second temporal trend have relatively high concentrations in the mid-morning through afternoon hours on weekdays and afternoon hours on weekend. These areas include industrial and residential sites in the northeast corner of West Oakland. While our model is specific to West Oakland and the 100×100 campaign, we expect that a similar approach would successful in other locales with similar intensive monitoring data.

Recognizing that the 100×100 campaign was a unique opportunity to conduct intensive spatiotemporal monitoring in an urban region, it is important to understand whether similar modeling results can be obtained with less intensive monitoring. The subsampling simulation demonstrates that it is possible to leverage spatially dense observations from a short-term monitoring campaign to make accurate predictions at a time with more limited spatially sparse monitoring. In practice, this suggests that it is feasible to use a short-term monitoring campaign to improve long term predictions in areas that are not near continuously operated monitors. For example, one could design a future monitoring campaign that includes 30 fixed sites over an entire 12 month time period and either another 70 monitors that are only deployed for a few shorter 1 month periods or another 10–20 monitors that are rotated through additional locations for 1 month at a time. Either design would be less operationally expensive than continuous deployment of 100 monitors for the full period and our results suggest they could result in similar model prediction accuracy across the full region.

Additional gains in prediction accuracy might be possible if a future campaign takes advantage of optimal monitor location-allocation strategies[28], potentially modified to accommodate temporally varying network size. A recently developed algorithm for real-time spatiotemporal monitor allocation[29] may be helpful, although with such an approach it will be important to consider the impact of preferential spatial sampling on inference[30,31], If the air pollution surface is to be used as the exposure in an epidemiological analysis, then consideration should also be given to compatibility between monitor and main study locations[32]. Another promising strategy is mobile monitoring, which can cover a much larger number of locations than fixed monitoring over an extended period of time, albeit with temporally sparse coverage[16]. Data from mobile monitoring campaigns has been used successfully to fit spatial air pollution models[15,17,33]. It may be possible to incorporate mobile monitoring data in a spatiotemporal model like the one described here, especially if it can be calibrated and included in a model with continuous fixed site monitoring at a modest number of locations[27].

4 Conclusion

We have utilized a geostatistical spatiotemporal model applied to data from to 100×100 campaign to predict hourly BC concentrations at all locations in West Oakland during the summer of 2017. These predictions provide insights into the complex spatially varying temporal air pollution trends and how they relate to local sources and neighborhood factors. Our subsampling analysis demonstrates that this modeling strategy can be employed to get similar prediction accuracy even with a less intense monitoring campaign in which some monitors are in service for only part of the modeled period. Future research is needed to determine optimal monitor placement strategies that will make it feasible to develop similar high resolution spatiotemporal air pollution predictions in other locations and over longer time periods.

Acknowledgments

We gratefully acknowledge the contribution of Ramon Alvarez from Environmental Defense Fund for his critical insights on all aspects of this research. We are grateful to Phil Martin and Steven Randall at the Bay Area Air Quality Management District and to Ms.

Margaret Gordon and Brian Beveridge at the West Oakland Environmental Indicators Project. This study was supported by a gift to Environmental Defense Fund from Signe Ostby and Scott Cook, Valhalla Foundation. TWK was supported by Department of Energy under Contract No. DEAC02-05CH11231.

References

1. US EPA National Center for Environmental Assessment RTPN, Sacks J. Integrated Science Assessment (ISA) for Particulate Matter (Final Report, Dec 2019) [Internet]. [cited 2021 Aug 2]. Available from: https://cfpub.epa.gov/ncea/isa/recordisplay.cfm?deid=347534

2. Liu C, Chen R, Sera F, Vicedo-Cabrera AM, Guo Y, Tong S, Coelho MSZS, Saldiva PHN, Lavigne E, Matus P, Valdes Ortega N, Osorio Garcia S, Pascal M, Stafoggia M, Scortichini M, Hashizume M, Honda Y, Hurtado-Díaz M, Cruz J, Nunes B, Teixeira JP, Kim H, Tobias A, Íñiguez C, Forsberg B, Åström C, Ragettli MS, Guo Y-L, Chen B-Y, Bell ML, Wright CY, Scovronick N, Garland RM, Milojevic A, Kyselý J, Urban A, Orru H, Indermitte E, Jaakkola JJK, Ryti NRI, Katsouyanni K, Analitis A, Zanobetti A, Schwartz J, Chen J, Wu T, Cohen A, Gasparrini A, Kan H. Ambient Particulate Air Pollution and Daily Mortality in 652 Cities. N Engl J Med. Massachusetts Medical Society; 2019 Aug 22;381(8):705–715. PMID: 31433918

3. Dominici F, Peng RD, Bell ML, Pham L, McDermott A, Zeger SL, Samet JM. Fine particulate air pollution and hospital admission for cardiovascular and respiratory diseases. JAMA. 2006 Mar 8;295(10):1127–1134. PMCID: PMC3543154

4. Marshall JD, Nethery E, Brauer M. Within-urban variability in ambient air pollution: Comparison of estimation methods. Atmos Environ. 2008 Feb 1;42(6):1359–1369.

5. Jerrett M, Arain A, Kanaroglou P, Beckerman B, Potoglou D, Sahsuvaroglu T, Morrison J, Giovis C. A review and evaluation of intraurban air pollution exposure models. J Expo Sci Environ Epidemiol. Nature Publishing Group; 2005 Mar;15(2):185–204.

6. Hoek G, Beelen R, de Hoogh K, Vienneau D, Gulliver J, Fischer P, Briggs D. A review of land-use regression models to assess spatial variation of outdoor air pollution. Atmos Environ. 2008 Oct 1;42(33):7561–7578.

7. Mercer LD, Szpiro AA, Sheppard L, Lindström J, Adar SD, Allen RW, Avol EL, Oron AP, Larson T, Liu L-JS, Kaufman JD. Comparing universal kriging and land-use regression for predicting concentrations of gaseous oxides of nitrogen (NOx) for the Multi-Ethnic Study of Atherosclerosis and Air Pollution (MESA Air). Atmospheric Environ Oxf Engl 1994. 2011 Aug 1;45(26):4412–4420. PMCID: PMC3146303

8. Su JG, Jerrett M, Beckerman B, Wilhelm M, Ghosh JK, Ritz B. Predicting traffic-related air pollution in Los Angeles using a distance decay regression selection strategy. Environ Res. 2009 Aug 1;109(6):657–670.

9. Su JG, Brauer M, Ainslie B, Steyn D, Larson T, Buzzelli M. An innovative land use regression model incorporating meteorology for exposure analysis. Sci Total Environ. 2008 Feb 15;390(2):520–529.

10. Beelen R, Hoek G, Vienneau D, Eeftens M, Dimakopoulou K, Pedeli X, Tsai M-Y, Künzli N, Schikowski T, Marcon A, Eriksen KT, Raaschou-Nielsen O, Stephanou E, Patelarou E, Lanki T, Yli-Tuomi T, Declercq C, Falq G, Stempfelet M, Birk M, Cyrys J, von Klot S, Nádor G, Varró MJ, Dėdelė A, Gražulevičienė R, Mölter A, Lindley S, Madsen C, Cesaroni G, Ranzi A, Badaloni C, Hoffmann B, Nonnemacher M, Krämer U, Kuhlbusch T, Cirach M, de Nazelle A, Nieuwenhuijsen M, Bellander T, Korek M, Olsson D, Strömgren M, Dons E, Jerrett M, Fischer P, Wang M, Brunekreef B, de Hoogh K. Development of NO2 and NOx land use regression models for estimating air pollution exposure in 36 study areas in Europe – The ESCAPE project. Atmos Environ. 2013 Jun 1;72:10–23.

11. Abernethy RC, Allen RW, McKendry IG, Brauer M. A Land Use Regression Model for Ultrafine Particles in Vancouver, Canada. Environ Sci Technol. American Chemical Society; 2013 May 21;47(10):5217–5225.

12. Jerrett M, Burnett RT, Ma R, Pope CA, Krewski D, Newbold KB, Thurston G, Shi Y, Finkelstein N, Calle EE, Thun MJ. Spatial Analysis of Air Pollution and Mortality in Los Angeles. Epidemiology. Lippincott Williams & Wilkins; 2005;16(6):727–736.

13. Zhang K, Larson TV, Gassett A, Szpiro AA, Daviglus M, Burke GL, Kaufman JD, Adar SD. Characterizing spatial patterns of airborne coarse particulate (PM10-2.5) mass and chemical components in three cities: the multi-ethnic study of atherosclerosis. Environ Health Perspect. 2014 Aug;122(8):823–830. PMCID: PMC4123025

14. Xu S, Zou B, Lin Y, Zhao X, Li S, Hu C. Strategies of method selection for fine-scale $PM_{2.5}$ mapping in an intra-urban area using crowdsourced monitoring. Atmospheric Meas Tech. Copernicus GmbH; 2019 May 28;12(5):2933–2948.

15. Messier KP, Chambliss SE, Gani S, Alvarez R, Brauer M, Choi JJ, Hamburg SP, Kerckhoffs J, LaFranchi B, Lunden MM, Marshall JD, Portier CJ, Roy A, Szpiro AA, Vermeulen RCH, Apte JS. Mapping Air Pollution with Google Street View Cars: Efficient Approaches with Mobile Monitoring and Land Use Regression. Environ Sci Technol. 2018 Nov 6;52(21):12563–12572. PMID: 30354135

16. Apte JS, Messier KP, Gani S, Brauer M, Kirchstetter TW, Lunden MM, Marshall JD, Portier CJ, Vermeulen RCH, Hamburg SP. High-Resolution Air Pollution Mapping with Google Street View Cars: Exploiting Big Data. Environ Sci Technol. 2017 Jun 20;51(12):6999–7008. PMID: 28578585

17. Kerckhoffs J, Hoek G, Messier KP, Brunekreef B, Meliefste K, Klompmaker JO, Vermeulen R. Comparison of Ultrafine Particle and Black Carbon Concentration Predictions from a Mobile and Short-Term Stationary Land-Use Regression Model. Environ Sci Technol. American Chemical Society; 2016 Dec 6;50(23):12894–12902.

18. Hankey S, Marshall JD. Land Use Regression Models of On-Road Particulate Air Pollution (Particle Number, Black Carbon, PM2.5, Particle Size) Using Mobile Monitoring. Environ Sci Technol. American Chemical Society; 2015 Aug 4;49(15):9194–9202.

19. Keller JP, Olives C, Kim S-Y, Sheppard L, Sampson PD, Szpiro AA, Oron AP, Lindström J, Vedal S, Kaufman JD. A unified spatiotemporal modeling approach for predicting concentrations of multiple air pollutants in the multi-ethnic study of atherosclerosis and air pollution. Environ Health Perspect. 2015 Apr;123(4):301–309. PMCID: PMC4384200

20. Szpiro AA, Sampson PD, Sheppard L, Lumley T, Adar SD, Kaufman JD. Predicting intra-urban variation in air pollution concentrations with complex spatio-temporal dependencies. Environmetrics. 2010;21(6):606–631.

21. Dons E, Van Poppel M, Kochan B, Wets G, Int Panis L. Modeling temporal and spatial variability of traffic-related air pollution: Hourly land use regression models for black carbon. Atmos Environ. 2013 Aug 1;74:237–246.

22. Caubel J, Cados T, Kirchstetter T. A New Black Carbon Sensor for Dense Air Quality Monitoring Networks. Sensors. 2018;

23. Caubel JJ, Cados TE, Preble CV, Kirchstetter TW. A Distributed Network of 100 Black Carbon Sensors for 100 Days of Air Quality Monitoring in West Oakland, California. Environ Sci Technol. American Chemical Society; 2019 Jul 2;53(13):7564–7573.

24. Sampson PD, Szpiro AA, Sheppard L, Lindström J, Kaufman JD. Pragmatic estimation of a spatio-temporal air quality model with irregular monitoring data. Atmos Environ. 2011 Nov 1;45(36):6593–6606.

25. Lindström J, Szpiro AA, Sampson PD, Oron AP, Richards M, Larson TV, Sheppard L. A Flexible Spatio-Temporal Model for Air Pollution with Spatial and Spatio-Temporal Covariates. Environ Ecol Stat. 2014 Sep;21(3):411–433. PMCID: PMC4174563

26. Finkenstadt B, Held L, Isham V, editors. Using Transforms to Analyze Space-Time Processes. Stat Methods Spatio-Temporal Syst. Chapman and Hall/CRC; 2006.

27. Chambliss SE, Preble CV, Caubel JJ, Cados T, Messier KP, Alvarez RA, LaFranchi B, Lunden M, Marshall JD, Szpiro AA, Kirchstetter TW, Apte JS. Comparison of Mobile and Fixed-Site Black Carbon Measurements for High-Resolution Urban Pollution Mapping. Environ Sci Technol. 2020 Jul 7;54(13):7848–7857. PMID: 32525662

28. Kanaroglou PS, Jerrett M, Morrison J, Beckerman B, Arain MA, Gilbert NL, Brook JR. Establishing an air pollution monitoring network for intra-urban population exposure assessment: A location-allocation approach. Atmos Environ. 2005 Apr 1;39(13):2399–2409.

29. Mukherjee R, Diwekar UM, Kumar N. Real-time optimal spatiotemporal sensor placement for monitoring air pollutants. Clean Technol Environ Policy. 2020 Dec 1;22(10):2091–2105.

30. Diggle PJ, Menezes R, Su T. Geostatistical inference under preferential sampling. J R Stat Soc Ser C Appl Stat. 2010;59(2):191–232.

31. Lee A, Szpiro A, Kim SY, Sheppard L. Impact of preferential sampling on exposure prediction and health effect inference in the context of air pollution epidemiology. Environmetrics. 2015 Jun;26(4):255–267. PMCID: PMC5863931

32. Szpiro AA, Paciorek CJ. Measurement error in two-stage analyses, with application to air pollution epidemiology. Environmetrics. 2013 Dec 1;24(8):501–517. PMCID: PMC3994141

33. Kerckhoffs J, Hoek G, Gehring U, Vermeulen R. Modelling nationwide spatial variation of ultrafine particles based on mobile monitoring. Environ Int. 2021 Sep 1;154:106569.

Figure 1: Systematic time trends from the spatio-temporal model: The area-wide average and both temporal basis functions, $f_1(t)$ and $f_2(t)$, shown on different time scales, (top) hourly scale over the full monitoring period, (middle left) average diurnal trend over weekdays, (middle right) average diurnal trend over weekends, (bottom left) average calendar week summarized by daily averages, and (bottom right) average calendar week summarized by hourly averages. In each panel, the red line shows the absolute value of the area-wide average concentration, and the blue and green lines show the relative differences compared to the area-wide average that are multiplied by the site-specific values of Beta1 and Beta2, respectively.

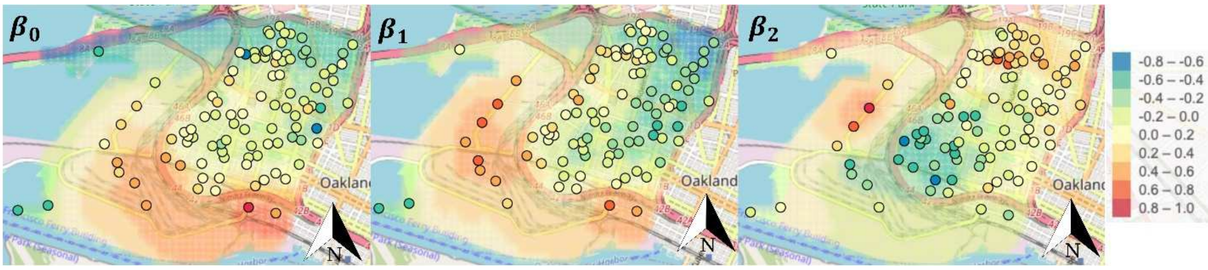

Figure 2 β-fields from the spatio-temporal model, where points indicate estimated values at observed locations. Beta 0 corresponds to the difference in BC concentration from the area-wide average at each location. Beta 1 and Beta 2 are coefficients for the respective temporal basis function shown in Figure 1. Note that the relative contribution of the area-wide average and the two temporal basis functions to the overall time series at each location differs across the domain. Coefficients near zero reflect locations where a specific temporal pattern has relatively little influence on the concentration time-series, where coefficients with higher absolute value reflect locales where the relative contribution of a temporal pattern is higher.

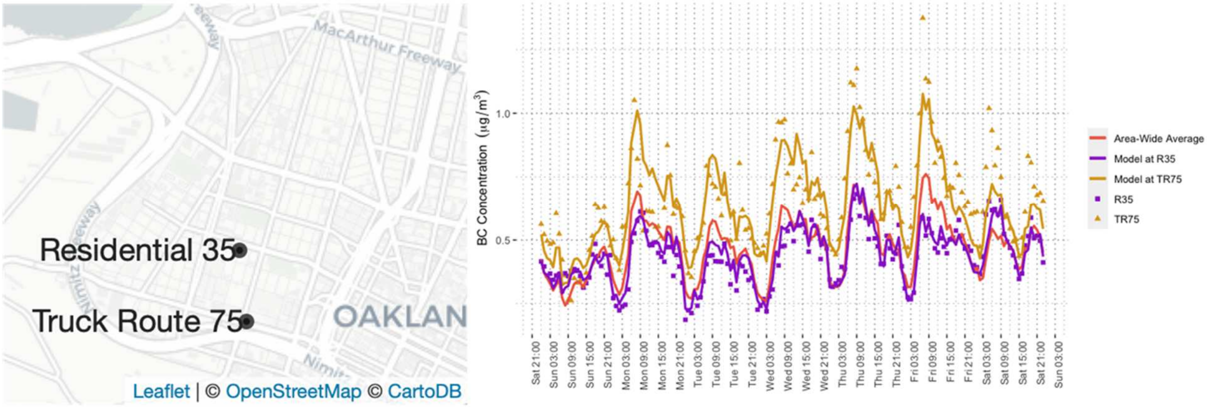

Figure 3: BC concentrations at example community sites Residential 35 (R35) and Truck Route 75 (TR75). Left: Locations of Residential 35 and Truck Route 75, Right: Points show observed averages for each hour over a calendar week, while lines show estimates using the spatio-temporal model against the area-wide average.

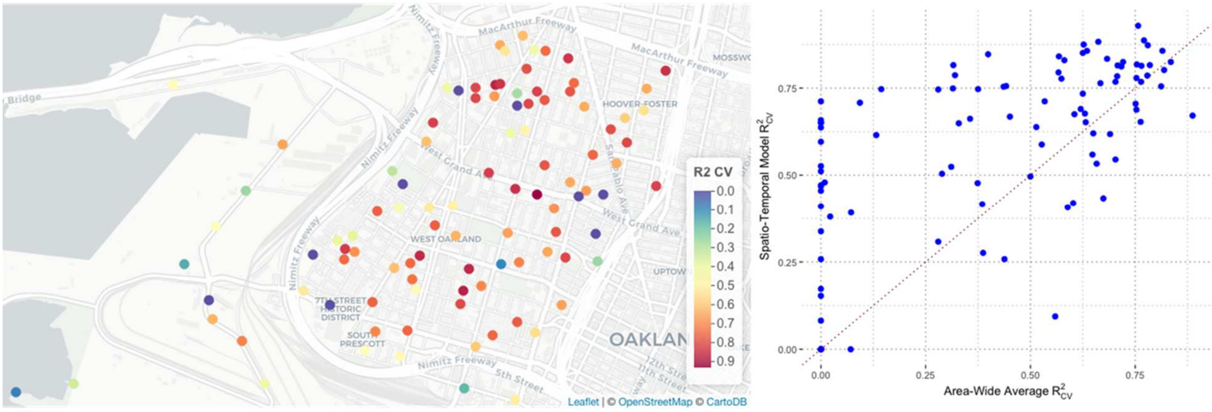

Figure 4: Prediction accuracy for each site from the 100×100 Network using the spatio-temporal model and the area-wide average. Reported R^2_{CV} is for a typical week. Left: R^2_{CV} for each site from the 100×100 Network. Right: R^2_{CV} compared at each site using the spatio-temporal model and the area-wide average.

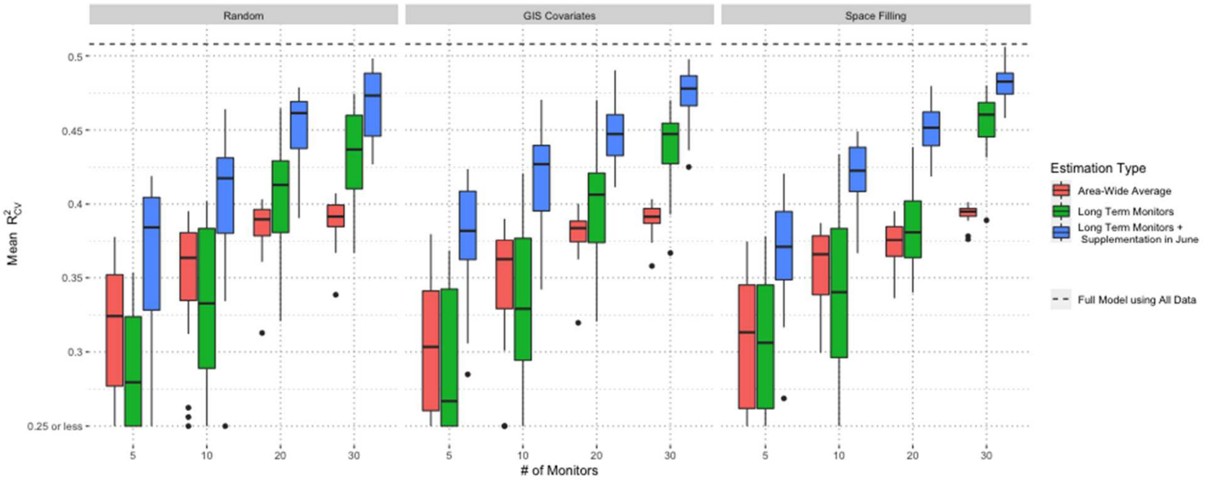

Figure 5: Cross-validated prediction accuracy on July data for each sub-sampled set of monitors. Area-wide average (orange) show prediction accuracy if no modeling was done and the surface was assumed to be constant across West Oakland. Long term monitors (Green) shows prediction accuracy from the spatio-temporal model without the supplementary monitoring in June. Long term monitors + supplement in June (Blue) shows prediction accuracy if short-term sampling is done at a large number of sites in June. The dotted line represents the best possible spatio-temporal model, where all data (including July) is used.